JOURNAL OF GEOPHYSICAL RESEARCH, VOL. 106, NO. D22, PAGES 28,771–28,784, NOVEMBER 27, 2001

Stratospheric N_2O–NO_y system: Testing uncertainties in a three-dimensional framework

S. C. Olsen,[1] C. A. McLinden,[2] and M. J. Prather

Department of Earth System Science, University of California at Irvine, Irvine, California, USA

Abstract. Nitrous oxide (N_2O) is an important greenhouse gas and the major source of stratospheric reactive nitrogen (NO_y), an active participant in the stratospheric chemistry controlling ozone depletion. Tropospheric N_2O abundances are increasing at nearly 0.3% yr^{-1} and this increase is expected to continue in the near future as are direct stratospheric NO_y perturbations, for example, from aircraft. In order to test and gain confidence in three-dimensional (3-D) model simulations of the stratospheric N_2O–NO_y system, a simplified photochemistry for N_2O and NO_y is developed for use in chemistry transport models (CTMs). This chemical model allows for extensive CTM simulations focusing on uncertainties in chemistry and transport. We compare 3-D model simulations with measurements and evaluate the effect on N_2O and NO_y of potential errors in model transport, in column and local ozone, and in stratospheric temperatures. For example, with the three different 3-D wind fields used here, modeled N_2O lifetimes vary from 173 to 115 years, and the unrealistically long lifetimes produce clear errors in equatorial N_2O profiles. The impact of Antarctic denitrification and an in situ atmospheric N_2O source are also evaluated. The modeled N_2O and NO_y distributions are obviously sensitive to model transport, particularly the strength of tropical upwelling in the stratosphere. Midlatitude, lower-stratospheric NO_y/N_2O correlations, including seasonal amplitudes, are well reproduced by the standard model when denitrification is included. These correlations are sensitive to changes in stratospheric chemistry but relatively insensitive to model transport. The lower stratospheric NO_y/N_2O correlation slope gives the correct net NO_y production of about 0.5 Tg N yr^{-1} (i.e., the cross-tropopause flux as in the Plumb-Ko relation) only when N_2O values from 250 to 310 ppb are used. As a consequence, the Synoz calibration of the flux of O_3 from the stratosphere to the troposphere needs to be corrected to 550 ± 140 Tg O_3 yr^{-1}.

1. Introduction

Stratospheric photochemistry couples nitrous oxide (N_2O) with the family of reactive nitrogen species (NO_y) and stratospheric ozone [*Crutzen*, 1971; *Johnston*, 1971]. Nitrous oxide is the third most important greenhouse gas in terms of direct anthropogenic emissions behind CO_2 and CH_4. Source strength estimates for N_2O range from 10 to 17 Tg N yr^{-1} with significant contributions from microbial processes in soils and oceans, biomass burning, and industrial processes. This gas is well mixed in the troposphere: mean abundances were about 314 ppb (mole fraction) in 1998 and are increasing at nearly 0.3% yr^{-1} [*Prinn and Zander*, 1999] chiefly as the result of anthropogenic nitrogen fixation [*Mosier et al.*, 1998]. N_2O has an atmospheric lifetime of approximately 120 years [*Prinn and Zander*, 1999] and is destroyed primarily in the stratosphere via photolysis or reaction with $O(^1D)$. One of the products of this latter reaction is NO, the primary source of stratospheric reactive nitrogen, NO_y (= N + NO + NO_2 + HNO_3 + $2\times N_2O_5$ + ...). NO_y compounds are active participants in ozone chemistry, including both catalyzed loss [*Crutzen*, 1971; *Johnston*, 1971] and production [*Haagen-Smit*, 1952], as well as interference with chlorine- and odd-hydrogen-catalyzed destruction [*Prather et al.*, 1979; *Wennberg et al.*, 1994]. NO_y is removed from the stratosphere either through reaction within the family between N and NO at high altitudes or through transport to the troposphere where it is deposited as nitrate compounds. Additionally, NO_y transport out of the stratosphere may be enhanced by denitrification processes in the winter polar vortex. The

[1]Now at Division of Geological and Planetary Science, California Institute of Technology, Pasadena, CA USA

[2]Now at Meteorological Service of Canada, Downsview, Ontario, Canada.

Paper number 2001JD000559.
0148-0227/01/2001JD000559$09.00

stratosphere-to-troposphere NO_y flux is estimated to be 0.4–0.8 Tg N yr^{-1} [*Murphy and Fahey*, 1994].

Accurate modeling of the N_2O–NO_y system today is a prerequisite to evaluating future changes from increased emissions of N_2O or direct perturbations to NO_y (e.g., from aircraft). A number of studies have been made with two-dimensional (2-D) models [*Rosenfield and Douglass*, 1998; *Nevison et al.*, 1997a, 1997b, 1999; *Vitt et al.*, 2000], and this work needs to be expanded and transferred to the three-dimensional (3-D) models that will be used in future assessments. A number of 3-D stratospheric models include full chemistry and would be capable of analyzing the stratospheric N_2O-NO_y system [e.g., *Kaminski et al.*, 1996; *Douglass et al.*, 1997; *Chipperfield*, 1999; *Riese et al.*, 2000; *van den Broek et al.*, 2000; *Kinnison et al.*, 2001]; however, the computational requirements for such models precludes multiyear, steady state simulations needed for sensitivity studies and error analyses. Thus we present here a simplified but accurate photochemical model for stratospheric N_2O and NO_y photochemistry that can be readily run as two simple tracers in a chemistry transport model (CTM). This paper focuses on uncertainties in chemistry and transport that would systematically alter simulated NO_y and hence O_3 abundances. It compares 3-D model simulations of the stratospheric N_2O–NO_y system with measurements to study the effect of potential errors in the dynamics and chemistry, in the assumptions of column ozone, in the climatology used for local ozone density, and in stratospheric temperatures. Three different meteorological fields are compared, but feedbacks on the O_3 and radiative forcing of the circulation are not considered. In each case the observational constraints can highlight model deficiencies and their cause. The Plumb-Ko relationship [*Plumb and Ko*, 1992] between the NO_y/N_2O correlation slope and their fluxes is tested. In addition, the impact of Antarctic denitrification and of possible stratospheric N_2O production from the reaction of excited NO_2 and N_2 [*Zellner et al.*, 1992] are evaluated in a 3-D model in the context of observational constraints.

2. Observations

Current observations of the stratospheric N_2O–NO_y system from satellites, aircraft, and balloons define some clear latitudinal, altitudinal, and seasonal features that models should be able to simulate. N_2O abundances in the stratosphere fall off with altitude and are pushed up higher in the tropics, producing hat-like contours with the brim dropping toward the poles. On the other hand, NO_y abundances peak in the tropical midstratosphere and fall off as one moves away from this region. In the lower stratosphere where N_2O and NO_y lifetimes are long compared to transport times, theory predicts [*Plumb and Ko.*, 1992] and observations confirm [*Fahey et al.*, 1990; *Lowenstein et al.*, 1993; *Fahey et al.*, 1996; *Keim et al.*, 1997] a compact linear correlation between NO_y and N_2O.

Observations from the NASA ER-2 missions (Airborne Southern Hemisphere Ozone Expedition/Measurements for Assessing the Effects of Stratospheric Aircraft (ASHOE/MAESA) and Stratospheric Tracers of Atmospheric Transport (STRAT)) show that in the Northern Hemisphere the correlation slope for potential temperatures > 400 K and N_2O > 150 ppb varies seasonally from -0.069 to -0.073, while in the Southern Hemisphere the seasonal variation is much larger, from -0.058 to -0.077 [*Keim et al.*, 1997]. The impact of Antarctic winter denitrification as a possible cause of this seasonality [*Fahey et al.*, 1990; *Lowenstein et al.*, 1993; *Fahey et al.*, 1996; *Keim et al.*, 1997; *Nevison et al.*, 1997b] is investigated below, including a full budget analysis for NO_y from the 3-D CTM.

A second diagnostic used to elucidate the seasonality of the correlation slope is the effective conversion efficiency, also known as F_{NO_y} [*Fahey et al.*, 1990; *Keim et al.*, 1997].

$$F_{NO_y} = \frac{NO_y - NO_{y\,\text{tropopause}}}{N_2O_{\text{tropopause}} - N_2O}. \quad (1)$$

F_{NO_y} is a measure of the net conversion efficiency of N_2O to NO_y integrated over the stratospheric history of an air parcel since it crossed the tropical tropopause. In regions where F_{NO_y} remains constant, a compact linear NO_y/N_2O relationship exists that passes through the point corresponding to the N_2O and NO_y abundances at the tropical tropopause.

3. University of California Irvine Chemistry Transport Model

The University of California Irvine (UCI) chemistry transport model (CTM) consists of a resolution-independent transport module driven by a meteorological data set consisting of winds, temperature, convection, precipitation, and boundary layer physics (i.e., met-fields). The CTM solves the continuity equations for chemically reactive tracers, computing the tracer changes due to advection, convection, emissions, and chemical production and loss, over the three-dimensional model grid. The tracer distribution in each grid box is represented as a three-dimensional second-order polynomial, including cross terms, and advection uses the second-order moments scheme [*Prather*, 1986]. Use of the second-order moments allows for improved resolution of the tracer mixing ratio and chemistry in the vertical dimension [*Hall and Prather*, 1995]. In these experiments the transport is driven with a single year of met-fields, recycled annually to steady state, from the Goddard Institute for Space Science (GISS) middle atmosphere general circulation model (GCM). To provide examples of different stratospheric transport, three different GISS GCM met-fields are used (see Figure 1).

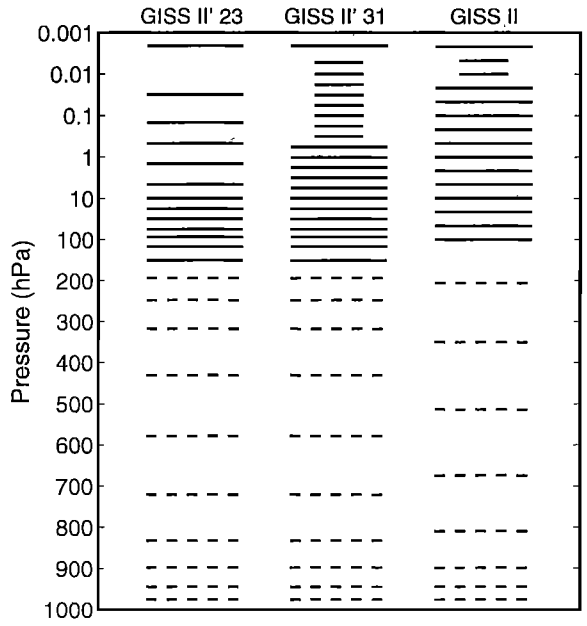

Figure 1. Vertical model level edges of the GISS-II′ 23L, GISS-II′ 31L, and GISS-II meteorological fields. Dashed lines indicate hybrid levels (using a surface pressure of 1000 hPa), and solid lines are constant pressure levels. Short solid lines indicate additional levels used by the GISS GCM but grouped together in the CTM (see text).

3.1. Meteorological Fields

The first meteorology is the archived output from the GISS model version II. It has a horizontal resolution of 7.8° latitude by 10° longitude and 23 vertical layers extending from the surface up to 0.002 mbar with approximately 5-km resolution in the stratosphere. The top three GCM layers are well mixed vertically on a timescale of months and have been combined to form a 21-layer CTM. The meteorological fluxes are archived at 8-hour intervals, and explicit horizontal diffusion is included only in the troposphere to correct for a too-sluggish interhemispheric transport in the GISS-II met-fields. This model has been used previously in studies of the Antarctic ozone hole [*Prather et al.*, 1990] and stratospheric tracer correlations [*Avallone and Prather*, 1997].

The second meteorology is based on the GISS model version II′ [*Koch and Rind*, 1998; *Rind and Lerner*, 1996]. It has a horizontal resolution of 4° latitude by 5° longitude and 31 vertical layers extending from the surface up to 0.002 mbar. The uppermost levels are, again, well mixed vertically on a timescale of months; and thus for use in the CTM the top eight layers have been combined into one with a mass-weighted mean altitude of about 58 km. This 23-layer CTM has approximately 4-km resolution in the middle stratosphere and 2-km resolution near the tropopause. The meteorological fluxes are archived at 6-hour intervals. This model has been used to study simplified interactive ozone parameterizations [*McLinden et al.*, 2000], and a 28-layer version of this model has been used to study the influx of extraterrestrial cometary water [*Hannegan et al.*, 1998].

The third meteorology is based on the GISS model version II′ with a horizontal resolution of 4° latitude by 5° longitude with 23 layers extending from the surface up to 0.002 mbar. This model has the same vertical structure as the 31-layer GCM from the surface to 10 mbar but fewer levels in the upper stratosphere and mesosphere. These met-fields are archived at 3-hour intervals. These three meteorological fields are referred to as the GISS-II, GISS-II′ 31L, and GISS-II′ 23L, respectively.

3.2. Chemistry Module

The chemistry module calculates loss frequencies, yields, and branching ratios based on the current atmosphere, adopting a monthly zonal mean climatology for ozone and temperature [*McPeters*, 1993; *Nagatani and Rosenfield*, 1993]. The production and loss of N_2O and NO_y in the CTM are computed from five tables of coefficients (designated C1 through C5 here) that are precalculated off-line in the UCI photochemical box model at 20 pressure altitudes from $z^* = 14$ km to 52 km in 2 km steps ($z^* = 16 \log_{10}(1000/p)$), 18 latitudes (85°S, 75°S, ..., 75°N, 85°N), and 12 months. The full tables are available from the authors, and a sample for January 5°N is given in Table 1.

The coefficients are mapped onto the CTM geographic grid and interpolated to the CTM vertical layers using the second-order moments, which are also utilized throughout the chemical calculations. For altitudes greater than 52 km, the 52-km values are used [*Hall and Prather*, 1995; *Avallone and Prather*, 1997; *Douglass et al.*, 1999]. Rate coefficients and photolysis cross sections are from Jet Propulsion Laboratory (*JPL*) *Publication 97-4* [*DeMore et al.*, 1997]. The transmission through the molecular oxygen Schumann-Runge (S-R) bands uses an opacity distribution function for each S-R band [*Fang et al.*, 1974] with updated, temperature-dependent cross sections [*Minschwaner et al.*, 1992]. The recent *JPL Publication 00-3* [*Sander et al.*, 2000] includes updates to some NO_y reactions as well as the new, long-wavelength tail in the $O(^1D)$ quantum yield. These changes have a negligible impact on the chemistry of the middle and upper stratosphere that controls the N_2O–NO_y system. In a sample sensitivity calculation with the GISS-II CTM, these JPL-00 revisions alter N_2O by 0.3 ppb (0.2%) and NO_y by 0.5 ppb (3%) in the tropical midstratosphere with considerably smaller changes elsewhere.

The relevant N_2O and NO_y photochemistry is shown in reactions (R1) to (R7). Reactions (R1) to (R3) describing N_2O loss and NO_y production depend on four atmospheric factors: (1) the local O_3 abundance, (2) and (3) the overhead O_2 and O_3 columns, and (4) the local temperature, all of which are prescribed in the cli-

Table 1. Sample of the N_2O-NO_y Linearized Chemistry Tables for the January 5°N Atmosphere.[a]

Altitude, km	C1	C2	C3	C4	C5
60	3.034E-07	2.204E-02	1.059E-06	2.916E+07	3.408E-04
58	3.004E-07	2.752E-02	9.346E-07	1.943E+07	5.247E-04
46	2.967E-07	3.400E-02	8.126E-07	1.329E+07	8.396E-04
54	2.913E-07	4.121E-02	6.959E-07	9.568E+06	1.401E-03
52	2.806E-07	4.915E-02	5.861E-07	8.532E+06	2.422E-03
50	2.691E-07	5.768E-02	4.835E-07	7.414E+06	4.384E-03
48	2.542E-07	6.618E-02	3.878E-07	6.782E+06	8.368E-03
46	2.329E-07	7 175E-02	2.997E-07	6.911E+06	1.682E-02
44	2.045E-07	7.172E-02	2.193E-07	7.709E+06	3.492E-02
42	1.703E-07	6.621E-02	1 478E-07	9.401E+06	7.067E-02
40	1.343E-07	5.895E-02	8.896E-08	1.225E+07	1.271E-01
38	1.005E-07	5.331E-02	4.761E-08	1.640E+07	1.938E-01
36	7.114E-08	5.018E-02	2.245E-08	2.165E+07	2.594E-01
34	4.733E-08	4.899E-02	9.049E-09	2.705E+07	3.177E-01
32	2.939E-08	4.966E-02	2.998E-09	3.060E+07	3.654E-01
30	1.698E-08	5.263E-02	8.046E-10	3.048E+07	4.016E-01
28	9.129E-09	5.827E-02	1.776E-10	2.776E+07	4.226E-01
26	4.612E-09	6.390E-02	3.682E-11	2.647E+07	4.119E-01
24	2.241E-09	6.354E-02	9.081E-12	3.192E+07	3.463E-01
22	1.055E-09	5.811E-02	2.873E-12	5.619E+07	2.343E-01
20	4.641E-10	5.500E-02	9.481E-13	1.381E+08	1.316E-01
18	1.812E-10	6.239E-02	2.082E-13	3.181E+08	7.703E-02
16	5.885E-11	8.703E-02	2.470E-14	4.312E+08	4.884E-02
14	1.640E-11	1.796E-01	1.225E-15	2.326E+08	4.124E-02

[a]Complete tables (18 latitudes by 12 months) are available from the authors. See text for definition of C1-C5. Read 3.034E-07 as 3.034×10^{-7}.

matology. The majority (90%) of N_2O is photolyzed (reaction (R1)), and the rest reacts with $O(^1D)$ with about 6% of the N from atmospheric N_2O producing NO_y. The first two chemistry tables are C1, the 24-hour average N_2O loss frequency (the sum of (R1) to (R3)), and C2, the fractional yield of NO from N_2O loss ((R3) divided by the total loss, reactions (R1)+(R2)+(R3)). These two coefficients are used to calculate the local N_2O loss and NO_y production in the CTM. They are independent of the local N_2O abundance and depend only on the photolysis frequencies of N_2O and O_3 plus the rate coefficients for reactions (R2) and (R3).

(R1) $N_2O + h\nu \rightarrow N_2 + O$ (~90%),
(R2) $N_2O + O(^1D) \rightarrow N_2 + O_2$ (~4%),
(R3) $N_2O + O(^1D) \rightarrow NO + NO$ (~6%).

The loss of NO_y (reactions (R4) to (R7)) depends on the local NO_y abundance as well as the four other atmospheric factors noted above. Most NO photolysis (reaction (R4)) occurs in the NO δ bands ($\lambda = 182-191$ nm), which overlap the O_2 Schumann-Runge bands [*Nicolet and Cieslik*, 1980], greatly complicating the photolysis calculations. The UCI box model uses opacity distribution functions for O_2 and mean band strengths for NO [*Fang et al.*, 1974; *Minschwaner and Siskind*, 1993] to calculate the NO photolysis rate. Most of the N released in reaction (R4) reforms NO (reaction (R5)), but a fraction proceeds via (R6) effectively removing two NO_y.

(R4) $NO + h\nu \rightarrow N + O$
(R5) $N + O_2 \rightarrow NO + O$ $k=1.5\text{x}10^{-11}e^{-3600/T}$,
(R6) $N + NO \rightarrow N_2 + O$ $k=2.1\text{x}10^{-11}e^{100/T}$,
(R7) $N + NO_2 \rightarrow N_2O + O$ $k=5.8\text{x}10^{-12}e^{220/T}$.

Table C3 is the 24-hour average NO photolysis frequency per NO_y molecule. This table effectively includes the diurnal average of the product of NO photolysis and the fraction of NO_y as NO. Thus the production of atomic N is calculated in the CTM as the abundance of NO_y times the frequency from table C3. The fourth table, C4, is used to calculate the fraction of atomic N reacting with NO (reaction (R6)) or NO_2 (reaction (R7)), thereby destroying two NO_y molecules, as opposed to that reacting with O_2 (reaction (R5)), regenerating NO_y. The coefficients in C4 are the ratio of the rates of (R6) plus (R7) to that of (R5) divided by the mixing ratio of NO_y (f_{NO_y}); this set of coefficients is thus independent of the NO_y distribution assumed in the climatology. The loss frequency of NO_y in the CTM, calculated as $2\times$ C3 $\times$ (C4 $\times f_{NO_y}$) /(1 + C4 $\times f_{NO_y}$), is nonlinear in the NO_y abundance. The small amount of N_2O formed by (R7) is tested with sensitivity studies here using a fifth table of coefficients C5, the fraction of NO_y loss that regenerates N_2O, that is, (R7)/((R6) + (R7)). These tables are available from the authors.

In all simulations the abundances in the lowest four model layers (about 0-2 km altitude) are relaxed to 310 ppb N_2O and 0.25 ppb NO_y with a 2-day e-folding time.

There is no flux across the top model boundary. The model is initialized with typical values and run for 10 model years to a near, annually repeating, steady state.

3.3. Alternative Chemistries

3.3.1. Ozone and temperature climatologies. In order to study the effects of possible errors in the ozone and temperature climatologies, model runs are performed with three new sets of tables, each one calculated from a slightly perturbed version of these climatologies. For the first set of tables the local O_3 density is increased uniformly by 10%, affecting the local chemical rate calculations but not the radiation field. In the second, the overhead column O_3 is increased by 10%, affecting the photolysis calculations by decreasing the penetration of the UV radiation field, but not the local O_3 density. In this way the effects of O_3 on photolysis rates and chemical rates may be studied separately. The third set of tables is calculated with a uniform temperature increase of 10°C and can be viewed as a sensitivity to systematic errors in GCM temperatures or to climate change [*Rosenfield and Douglass*, 1998]. In these and subsequent studies of alternate chemistries the GISS-II met-fields are used.

3.3.2. Mesospheric chemistry. *Nevison et al.* [1997a] report that many stratospheric model simulations produce high-altitude NO_y abundances that are much greater than observations, and they suggest that uncertainties in key photochemical rate constants may be responsible. We investigate one aspect of this hypothesis by adding more "mesospheric" chemistry to our basic set of stratospheric chemistry tables, expanding the photolysis and kinetics an additional scale height up to 60 km.

3.3.3. In situ N_2O sources. Although N_2O sources are generally believed to be located at or near the Earth's surface, there have been several studies, both theoretical and experimental, postulating the existence of in situ atmospheric N_2O sources [e.g., *Prasad*, 1981; *Zipf and Prasad*, 1998; *Zellner et al.*, 1992; *Dentener and Crutzen*, 1994]. Proposed mechanisms for the upper atmosphere are generally based on atmospheric N_2 reacting with an excited species. Two such reactions are based on the reactive collisional quenching of NO_2^* and NO_3^* as proposed by *Zellner et al.* [1992], whose laboratory results give N_2O yields of (0.014 ± 0.006) and (0.0004 ± 0.0002), respectively, per nondissociative photon absorption through the reactions

$$\text{(R8)} \qquad NO_2^* + N_2 \rightarrow N_2O + NO,$$
$$\text{(R9)} \qquad NO_3^* + N_2 \rightarrow N_2O + NO_2.$$

In the atmosphere (R8) should be dominant, and we simulate this source with a new table of coefficients calculated as the ratio of the NO_2 photolysis rate to the NO_y density. The model assumes a 24-hour photostationary state for a typical profile of NO_y and calculates the average rate of NO_2 photolysis which is then scaled linearly to the amount of NO_y in the CTM, thus capturing the seasonal and spatial distribution of NO_2^*. The ratio of dissociative to nondissociative absorption by NO_2 is derived for top-of-atmosphere conditions and an additional factor of 0.78 (the N_2 fraction of air) is included. NO_2^* has two electronically excited states with fluorescence lifetimes of approximately 30 μs and 115 μs [*Zellner et al.*, 1992] and a collisional lifetime of approximately 4.7 μs at 50 km. Combining these factors, we calculate an N_2O source table that is proportional to the local NO_y abundance.

3.3.4. Antarctic denitrification. To investigate the effect of Antarctic denitrification on the NO_y/N_2O correlation slope (a well-observed quantity), a simulated annually recurring denitrification event is implemented in the CTM. This crude denitrification method consists of removing 99% of the NO_y abundance every October 31 in altitudes from 11 to 32 km poleward of 63°S latitude. This provides a reasonable, albeit upper limit, to the observed denitrification [*Santee et al.*, 1999].

4. Modeled N_2O and NO_y With Different Met-Fields

For all three met-fields the modeled N_2O mixing ratios are nearly constant in the troposphere and decrease with height in the stratosphere as photochemical destruction increases. In the stratosphere, N_2O contours are pushed down in the winter high latitudes as low N_2O air following the pole-to-pole mesospheric circulation descends; see Figure 2 for the GISS-II simulation. Higher N_2O abundances in the tropical stratosphere relative to mid latitudes and high latitudes is indicative of N_2O-laden air following the Brewer-Dobson circulation: entering the stratosphere through the tropical tropopause, rising in the tropics, spreading throughout the stratosphere, then descending and reentering the troposphere at higher latitudes [*Brewer*, 1949]. Contours for both GISS-II′ simulations are flatter with latitude relative to GISS-II, particularly in the tropics and at higher altitudes (Figure 3). Changes in model physics and numerics between GISS-II and GISS-II′ appear to have altered vertical transport in the tropical middle stratosphere.

Modeled stratospheric NO_y abundances peak in the tropical upper stratosphere near the maximum of the source of NO_y. The NO_y abundance falls off above and poleward because of the photochemical loss of NO_y in the mesosphere. (If NO_y were conserved in the stratosphere, as is the case for inorganic chlorine (Cl_y), then the maxima would occur in the polar mesosphere.) NO_y is clearly driven by the pole-to-pole mesospheric circulation pattern (Figure 2). The NO_y maxima for all three met-fields (Figure 4) occur in the upper tropical stratosphere with typical magnitudes of about 19 ppb for both GISS-II′ simulations and 17 ppb for GISS-II. The GISS II′ simulations also have steeper falloff above their maxima at all latitudes relative to GISS-II.

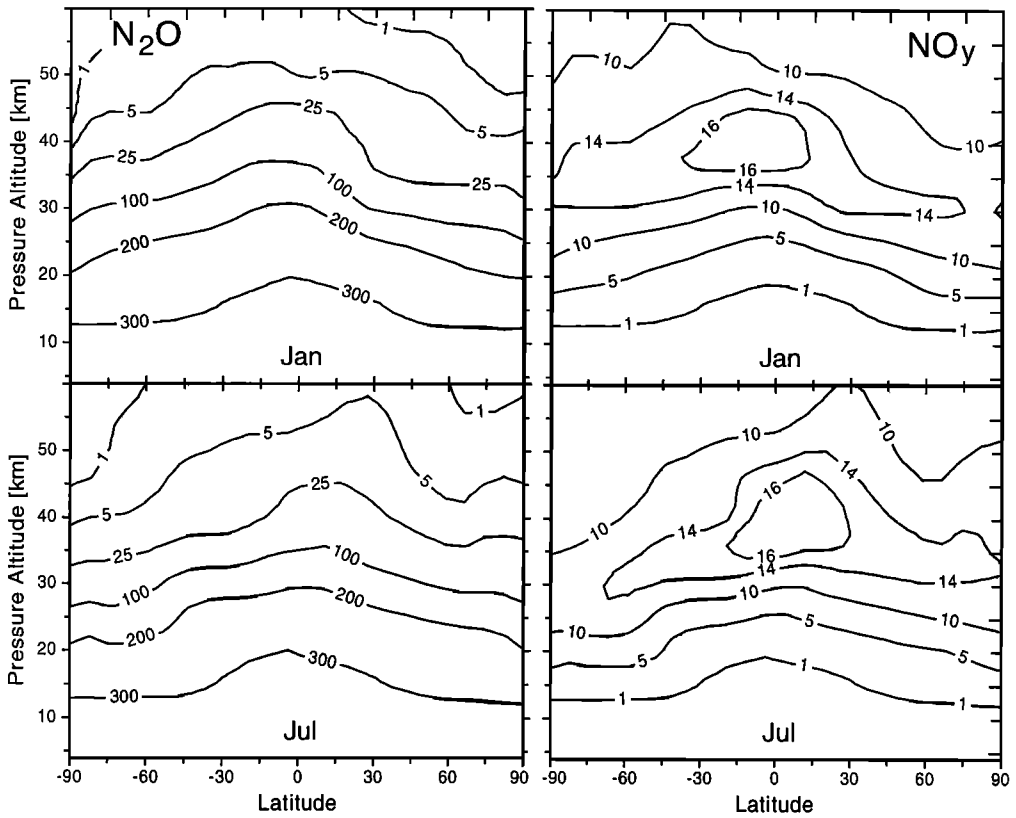

Figure 2. Zonal mean N_2O and NO_y mixing ratio (ppb) as a function of pressure altitude and latitude for January and July from the GISS-II model.

4.1. Comparison With Observations

There are a number of recent analyses and collations of stratospheric N_2O and NO_y measurements [e.g., *Michelsen et al.*, 1998; *Strahan*, 1999; *Danilin et al.*, 1999; *Santee et al.*, 1999]. This study is not meant to synthesize all of these, nor is it an exhaustive analysis of N_2O observations [e.g., *Roche et al.*, 1996] or simulations [e.g., *Douglass et al.*, 1999]. Rather, we focus on a few didactic examples where both N_2O and NO_y are measured. N_2O and the major reactive nitrogen species comprising NO_y are measured by the Atmospheric Trace Molecule Spectroscopy Experiment (ATMOS) [*Gunson et al.*, 1996]. Modeled N_2O and NO_y profiles are compared with these ATMOS measurements in Figures 5 and 6, respectively, for three different latitude bands and months.

For N_2O in the 10°S-10°N band the GISS-II profile matches the observations, but both GISS-II′ profiles are substantially (up to 50 ppb) below observations in the mid stratosphere and upper stratosphere. This region is particularly important since most N_2O loss occurs here. In the midlatitude bands (40°-50°, both N and S), however, all of the models generally overpredict N_2O in the lower stratosphere. Above 25 km the GISS-II model agrees well with ATMOS measurements at 40°-50°N while the GISS-II′ 23L model is in agreement with measurements at 40°-50°S.

For NO_y the GISS-II simulation reproduces the ATMOS 10°S-10°N NO_y profile faithfully up to its maximum (~17 ppb) near 37 km but is then larger than observations above. In contrast, both GISS-II′ profiles are pushed down in altitude, reaching their maxima about 5 km lower than that of the ATMOS profile. These simulations also overpredict NO_y above 50 km, although by about half as much as the GISS-II NO_y. In contrast, at the midlatitude bands there is less spread between the different modeled profiles, and they track the ATMOS profile fairly well up to about 45 km where, again, they all overpredict the NO_y abundance. Extending mesospheric NO_y chemistry above 52 km in these models improves the agreement, as discussed later.

Comparison with the observed NO_y/N_2O correlations reduces much of the tracer variability caused by transport; however, the correlation slope is an excellent diagnostic of the chemistry. There is generally good agreement between the model with all three met-fields and the ATMOS and ER-2 observations in the lower stratosphere at northern midlatitudes. Although modeled NO_y is slightly higher than observed for N_2O between 100 and 250 ppb, both models and measurements display tight, nearly linear relationships for N_2O abundances between 150 and 310 ppb (Figure 7). At higher altitudes the NO_y abundance turns over, peaking at N_2O values of about 70 ppb. The modeled NO_y/N_2O

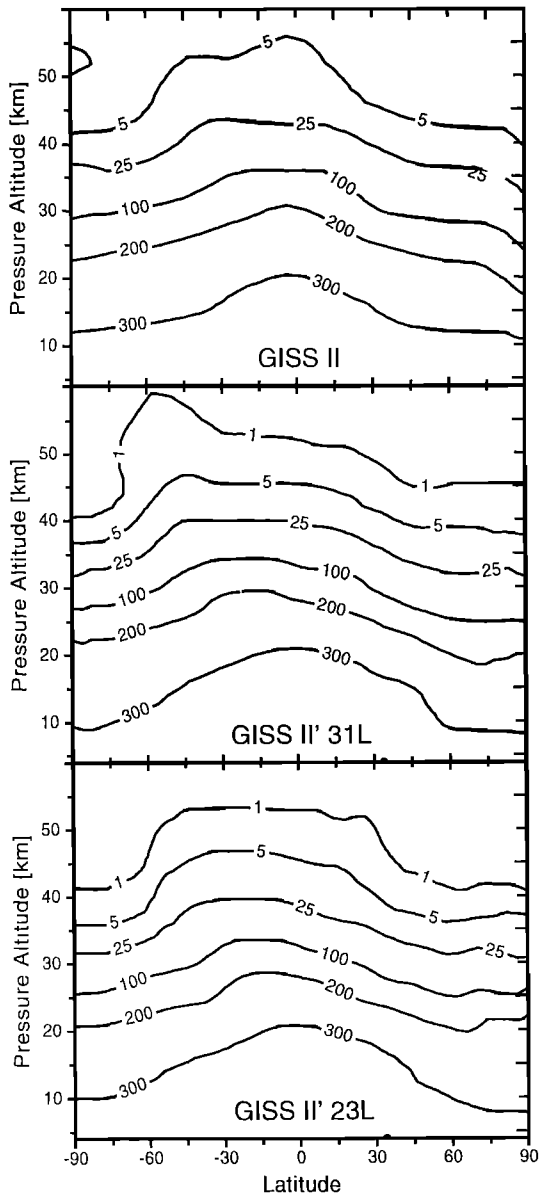

Figure 3. April zonal mean N_2O mixing ratio (ppb) as a function of pressure altitude and latitude for the GISS-II, GISS-II′ 31L, and GISS-II′ 23L models.

correlation plots for other regions (10°S-10°N and 40°S-50°S bands) are similar. The three different GISS metfields produce NO_y/N_2O plots that are remarkably similar, in spite of the large differences in the distribution of both N_2O and NO_y.

In the Northern Hemisphere the average NO_y/N_2O slope from GISS-II varies seasonally from -0.066 to -0.073 (calculated for N_2O values between 150 and 310 ppb and altitudes above 100 hPa). This slope is in excellent agreement with observations. In the Southern Hemisphere this standard model gives similar slopes, which are in marked contrast to observations showing a strong seasonality with much shallower slopes, -0.058, in Antarctic summer. This is attributed to Antarctic wintertime denitrification [e.g., *Nevison et al.*, 1997b] and is investigated with the 3-D CTM below.

4.2. Lifetimes and Source Strengths

There are large differences in the three models' N_2O source strengths and hence in their lifetimes (Table 2). The source strength is the total amount of N_2O added to maintain a 310 ppb mixing ratio in the lower troposphere, and the lifetime is calculated by dividing the atmospheric burden by this source strength. These differences are a direct consequence of the differences in the strength of the models' residual circulation. Both GISS-II′ models have relatively weak tropical upwelling as evident from the equatorial N_2O profiles (Figure 5, middle). With less N_2O in the upper stratosphere, where destruction is more rapid, these models have unrealistically long N_2O lifetimes (152 and 173 years for the GISS-II′ 31L and 23L, respectively). The GISS-II

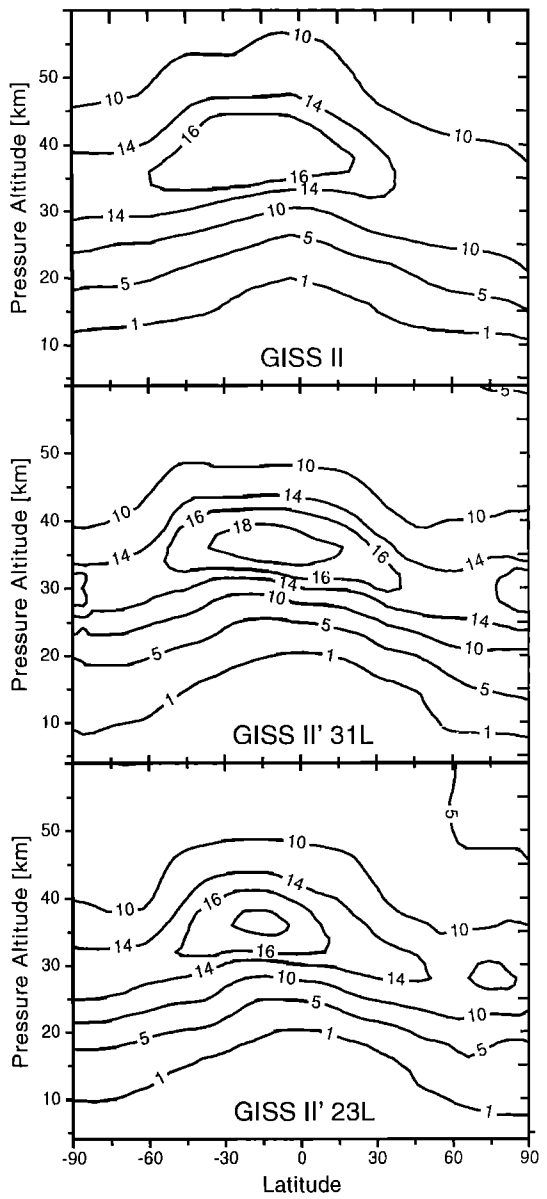

Figure 4. April zonal mean NO_y mixing ratio (ppb) as a function of pressure altitude and latitude for the GISS-II, GISS-II′ 31L, and GISS-II′ 23L models.

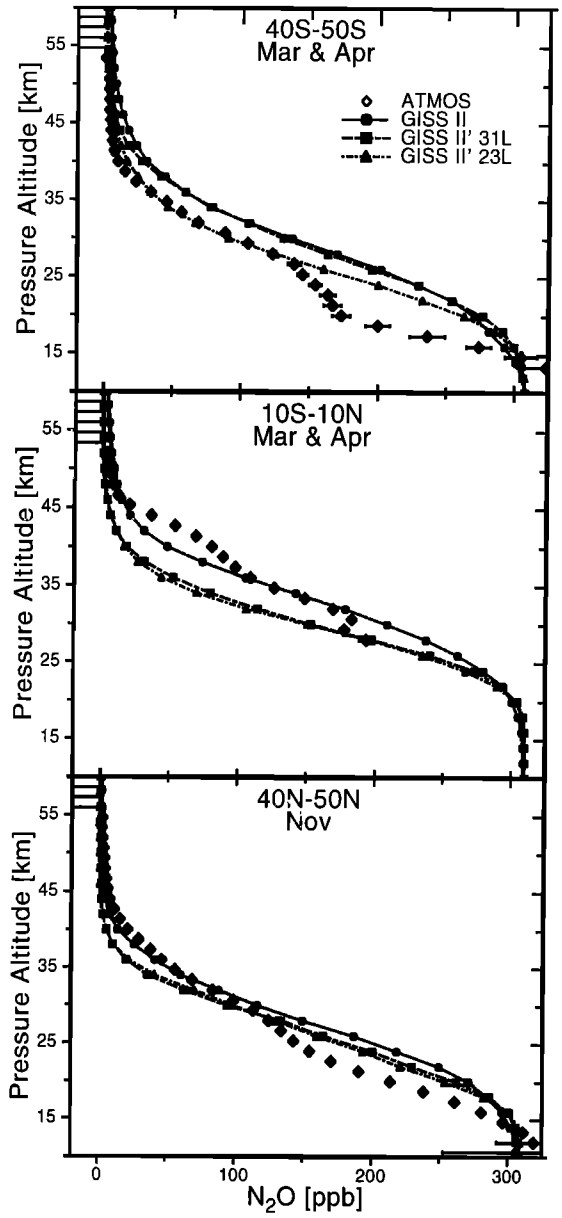

Figure 5. (top to bottom) N_2O vertical profiles (ppb) from the Atmospheric Trace Molecule Spectroscopy Experiment (ATMOS, open diamonds) and the GISS-II (dots), GISS-II′ 31L (squares), and GISS-II′ 23L (triangles) model simulations for latitude bands 40°S-50°S and 10°S-10°N in March and April and 40°N-50°N in November. Modeled data have been averaged over all longitudes and the latitude bands and months of the corresponding ATMOS measurements.

model has much stronger tropical upwelling, resulting in an N_2O lifetime (115 years) that is consistent with current best estimates (~120 years, [*Prinn and Zander*, 1999]). This analysis further supports the choice of an N_2O lifetime near 120 years since the GISS-II′ longer lifetimes are related to clear errors in their tropical profiles.

There is similarly a large range in modeled stratospheric NO_y source strengths and lifetimes. The NO_y lifetime is defined here using only the stratospheric NO_y burden and does not include tropospheric NO_y. The GISS-II flux agrees quite well with other estimates which range from 0.4 to 0.8 Tg N yr^{-1} [*Murphy and Fahey*, 1994], while the GISS-II′ fluxes are on the low side. Although the absolute cross-tropopause flux of NO_y varies between models, generally in proportion to the inverse of the N_2O lifetime, the fraction of the primary production of NO_y that is transported into the troposphere remains constant at about 70% with the remainder being lost to N+NO reactions in the upper stratosphere and mesosphere. Thus even for these three dramatically different stratospheric circulations the NO_y/N_2O correlation slopes remain nearly identical.

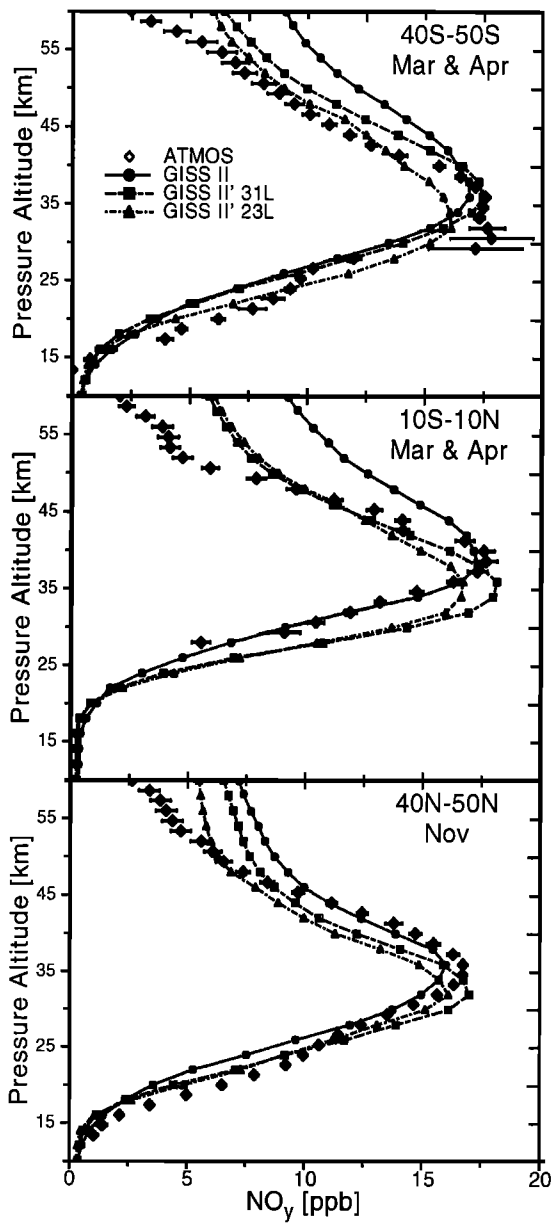

Figure 6. NO_y vertical profiles (ppb) from ATMOS and the GISS-II, GISS-II′ 31L, and GISS-II′ 23L model simulations. Symbols and regions as in Figure 5.

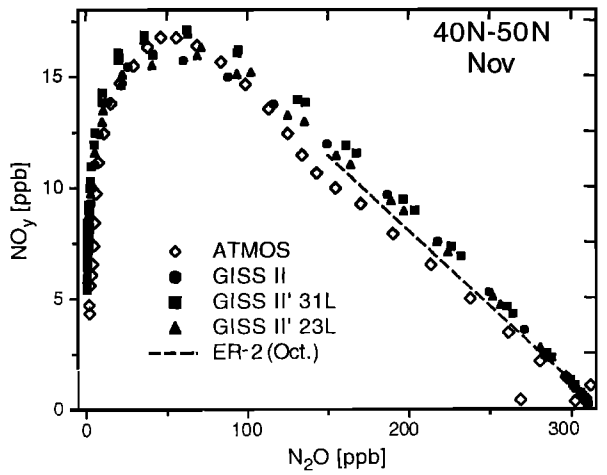

Figure 7. NO_y versus N_2O in the latitude band from 40°N to 50°N for November. Data are from the Atmospheric Trace Molecule Spectroscopy Experiment (ATMOS) and the GISS-II, GISS-II′ 31L, and GISS-II′ 23L model simulations and ER-2 aircraft. The ER-2 line is a least squares fit of Northern Hemisphere (18°N-60°N) data from October [*Keim et al.*, 1997]. Other symbols and data as in the bottom panels of Figures 5 and 6.

4.3. Correlations, Net Fluxes, and the Plumb-Ko Relationship

The Plumb-Ko relationship between the tracer correlation slopes and the relative fluxes across a mixing surface in the stratosphere [*Plumb and Ko*, 1992] provides a powerful tool for mapping observations onto fluxes, both for upward moving source gases [e.g., *Volk et al.*, 1997] and for the stratosphere-to-troposphere fluxes of NO_y and O_3 [*Murphy and Fahey*, 1994; *McLinden et al.*, 2000]. A 3-D model provides an ideal test bed to compare simulated tracer correlations and the exactly integrated fluxes.

The lower stratospheric NO_y/N_2O correlation slope is the observational measure of the net NO_y yield. Thus the modeled NO_y/N_2O correlation slope should equal the ratio of the stratosphere-to-troposphere NO_y flux to that of the N_2O stratospheric loss. The GISS-II simulation reproduces nearly the canonical "observed" average slope of -0.073 (from observations above 100 hPa and for N_2O between 150 and 310 ppb). Nevertheless, this value is not the same as the (negative) net yield calculated by the CTM. The NO_y and N_2O budgets indicate

Table 2a. Annual Mean N_2O and NO_y Budgets with Standard Chemistry Model and 310 ppb N_2O at Lower Boundary.

	GISS-II	GISS-II′ 31L	GISS-II′ 23L
1. N_2O lifetime, years	115.0	152.0	173.0
2 Tropospheric N_2O source, Tg N yr^{-1}	13.0	9.7	8.6
3 In situ N_2O source, Tg N yr^{-1}	...	...	...
4 Stratospheric NO_y lifetime, years	1.9	2.7	3.1
5. Stratospheric NO_y source, Tg N yr^{-1}	0.78	0 60	0.54
6. Stratospheric-Tropospheric NO_y flux, Tg N yr^{-1}	0.55	0.41	0.36
7 Dentrification, Tg N yr^{-1}	...	...	...
8 Percent N_2O loss yielding NO_y	6.0	6.2	6.3
9 Percent NO_y destroyed in stratosphere	30.0	32.0	33.0
10. Inferred net NO_y yield	0.085	0.085	0.084

Table 2b. Annual Mean N_2O and NO_y Budget Properties for Alternate Chemistries Using GISS-II Met-Fields.[a]

	Local O_3	Column O_3	Temperature	Mesospheric Chemistry	In Situ N_2O	Denitrify
1.	114.0	122.0	113.0	115.0	99.0	115.0
2.	13.0	12.3	13.2	13.0	9.8	13.0
3.	...	...	...	...	5.3	...
4.	1.9	2.0	2.0	1.9	1.8	1.8
5.	0.86	0.73	0.80	0.78	0.90	0.78
6.	0.61	0.52	0.61	0.55	0.61	0.48[b]
7.	...	...	...	...	...	0.09
8.	6.6	6.1	6.2	6.0	6.0[c]	6.0
9.	29.0	29.0	24.0	29.0	32.0	27.0
10.	0.094	0.087	0.094	0.085	0.081[c]	0.074

[a]Row numbers as in Table 2a. Column titles refer to 10% local ozone increase, 10% column ozone increase, 10°C temperature increase, mesospheric chemistry, in situ N_2O source, and Antarctic denitrification.

[b]Does not include denitrification flux to troposphere.

[c]Calculated using the total N_2O source.

that the correlation slope should be -0.085 (see Table 2a).

This discrepancy is resolved if one restricts the calculation of the slope to the extreme lower stratosphere. By selecting observations down to 180 hPa and with N_2O between 250 and 310 ppb, the simulated correlation slope is -0.83, in close agreement with the actual yield. Another clue pointing to this problem in picking such a wide N_2O range is that the intercept of the 150-310 ppb correlation line does not intersect with the tropospheric end points, whereas the 250-310 ppb correlation line does. Thus we conclude that the Plumb-Ko relationship holds but that the N_2O and NO_y are not in slope equilibrium over the range of 150 to 310 ppb N_2O and care must be taken when deriving empirical cross-tropopause fluxes.

4.4. Updated Stratosphere-Troposphere O_3 Flux

The original Synoz derivation of the cross-tropopause O_3 flux [*McLinden et al.*, 2000] was based on the following scaling: the steady state lifetime of N_2O is 120 (±17%) years and hence the flux of N_2O into the stratosphere is 0.45 (±17%) Tmoles yr^{-1}; the observed NO_y/N_2O slope in the midlatitude stratosphere is -0.073 (±14%) and hence the flux of NO_y out of the stratosphere is 0.46 Tg N yr^{-1}; the observed ratio NO_y/O_3 in the mid-latitude stratosphere is 0.0033 (±12%) and hence the flux of O_3 out of the stratosphere is 475 ± 120 Tg O_3 yr^{-1}. This work notes that the observed NO_y/N_2O slope in the midlatitude stratosphere is actually -0.085 in the lowermost stratosphere (i.e., when only N_2O data between 250 and 310 ppb are used) and that this value is consistent with the relative fluxes of N_2O and NO_y in a 3-D model that reproduces the observed curvature of the tracer correlation. Thus the corrected values for the stratospheric influx of NO_y is 0.53 Tg N yr^{-1}, and that of O_3 is 550 ± 140 Tg O_3 yr^{-1}.

5. Sensitivity to Alternative Chemistries

5.1. Ozone and Temperature Climatologies

5.1.1. Sensitivity to local ozone. The 10% increase in local O_3 density increases many chemical rates throughout the stratosphere (while leaving photolysis rates fixed). It has a negligible effect on N_2O abundances, decreasing N_2O by less than 1 ppb in the tropical midstratosphere (Figure 8). NO_y mixing ratios, however, are about 1.5 ppb (8%) greater than the standard run at 37 km. This might be expected since increased local O_3 leads to more $O(^1D)$, which produces more NO_y (reaction (R3)). The increase in stratospheric NO_y is evident in the NO_y/N_2O correlation plot, steepening the January lower stratospheric slope from -0.071 to -0.077 (Figure 9b versus the standard model in Figure 9a). Compared with the standard model, the N_2O lifetime and source strength are

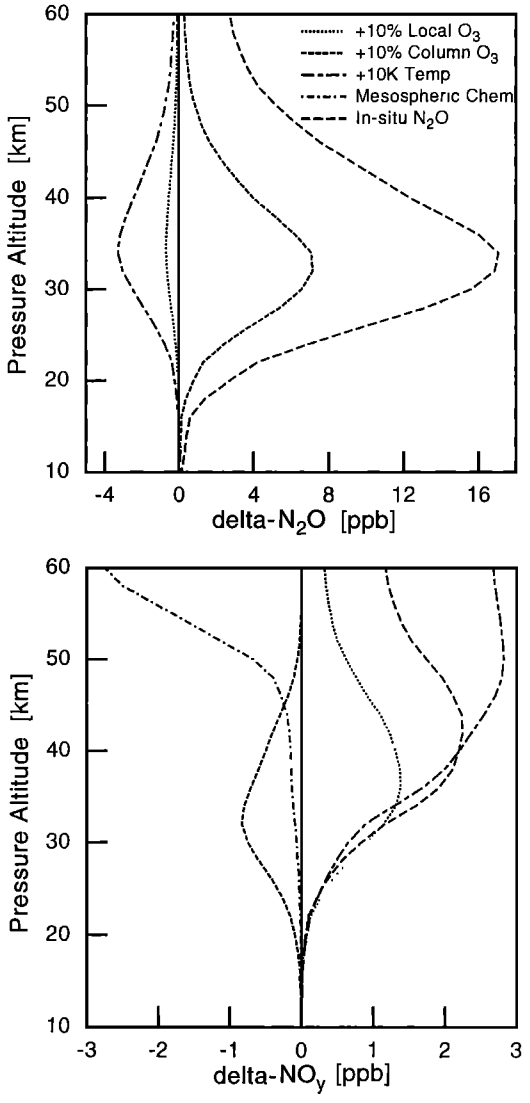

Figure 8. Equatorial (10°S-10°N) (top) N_2O and (bottom) NO_y zonal mean, annual average differences (ppb) between alternate and standard chemistry runs. GISS-II model results are shown for a uniform 10% local ozone increase (dotted line), a uniform 10% column ozone increase (short dash), a uniform 10°C temperature increase (long dash-short dash), mesospheric chemistry (short dash-dot, not visible on N_2O plot), and an in situ stratospheric N_2O source (long dash). Zero line (solid) is shown for reference.

relatively unaffected, while the NO_y primary source increases by about 10% (see Table 2b). There is correspondingly an increase in net NO_y yield and hence the stratosphere-to-troposphere NO_y flux.

5.1.2. Sensitivity to column ozone. The 10% increase in O_3 column reduces photolysis rates throughout the stratosphere. As a result, N_2O increases by about 7 ppb at 32 km, while NO_y decreases by 1 ppb (see Figure 8). In terms of NO_y the reductions in $O(^1D)$, and hence NO_y production, more than offset the increase in N_2O. These absolute differences become very small above 50 km and below 20 km. The NO_y/N_2O correlation slope in the January lower

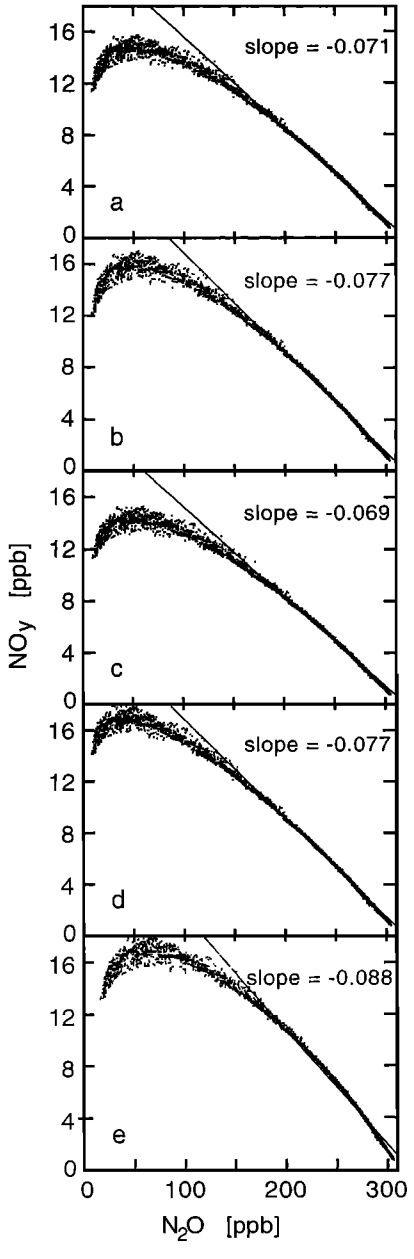

Figure 9. GISS-II modeled NO_y–N_2O correlation plots (ppb) of data from the region bounded by 24°N to 64°N latitude, 16 to 37 km altitude, and all longitudes for January. a) Standard chemistry, b) uniform 10% local ozone increase, c) uniform 10% column ozone increase, d) uniform 10°C temperature increase, and e) in situ atmospheric N_2O source. NO_y–N_2O slopes are least squares fits for data points with N_2O greater than 150 ppb.

stratosphere shifts slightly from -0.071 to -0.069 (Figure 9c). The N_2O lifetime increases slightly (6%), and the stratospheric NO_y source and stratosphere-troposphere flux decrease proportionately.

5.1.3. Sensitivity to temperature. The 10°C temperature increase alters the kinetic rate coefficients for many reactions and leads to about 3 ppb lower N_2O abundance in the midstratosphere. The NO_y increase is relatively much larger, about 3 ppb above 45 km in equatorial regions and persists through all seasons. The high temperature sensitivity of NO_y is due to the large increase in rate coefficient for (R5) with temperature and its affect on the branching ratio for N atoms between (R5) and (R6). This result is consistent with previous reports of NO_y decreases associated with a 10°C temperature decrease resulting from the doubling of atmospheric CO_2 in a 2-D coupled chemistry and dynamics model [*Rosenfield and Douglass*, 1998]. This reduced loss of NO_y in the upper stratosphere steepens the lower stratospheric correlation slope to -0.077 (Figure 9d), similar to the local O_3 increase, although peak NO_y abundances are higher. The N_2O budget is largely unaffected, and the primary source of NO_y increases by only 3%. The net NO_y flux, however, increases by approximately 10% because a smaller fraction of NO_y is destroyed in the upper atmosphere.

5.2. Mesospheric Chemistry

The inclusion of lower mesospheric chemistry has a large impact on modeled NO_y abundances above 45 km but no effect on N_2O (Figure 8). Between 50 and 60 km the difference increases with altitude until at 60 km the NO_y abundance is nearly 3 ppb less than in the standard chemistry. Thus mesospheric chemistry brings the model profile into much better agreement with ATMOS observations; however, the model still overpredicts NO_y abundances at 55 km. There is no effect on the global budgets of either N_2O or NO_y. Clearly, the standard NO_y chemistry as calculated here should be extended to 60 km and above, and then it may be possible to match the observed NO_y abundances above 45 km.

5.3. In Situ N_2O Source

The presence of an in situ stratospheric N_2O source would have implications for the tropospheric source strength and isotopomer composition. It would also complicate the definition of the N_2O lifetime. While the impact of stratospheric sources was briefly noted in a 2-D study [*Newson et al.*, 1999], we examine here in the 3-D model a spatially resolved source based on the *Zellner et al.* [1992] mechanism. At steady state the source of N_2O from (R8) within the stratosphere is 5.3 Tg N yr^{-1}. Because this source is located in the stratosphere where it is more rapidly removed, it offsets only 3.2 Tg N yr^{-1} of the tropospheric source. A new tropospheric source of magnitude 3 Tg N yr^{-1}, is barely possible within the current uncertainty of the N_2O budget [*Mosier et al.*, 1998]. Technically, the global mean lifetime of N_2O decreases to 99 years, in spite of no change in the photochemical loss processes, since the in situ source is in a region of active N_2O destruction. This shift emphasizes the fact that the atmospheric lifetime of even a long-lived gas like N_2O can depend on the distribution of sources [*Prather*, 1998]. The production of stratospheric NO_y increases by 15% while the stratosphere-troposphere NO_y flux increases by only

10% since a higher percentage of NO_y is destroyed in the upper stratosphere.

There are, however, substantial changes in stratospheric N_2O and NO_y patterns (Figure 8). Annual mean tropical N_2O abundances are over 16 ppb higher at 35 km than in the standard model. The increase in N_2O is highly seasonal, reaching its maxima following the long days of polar summer when the in situ source is greatest. For example, the model predicts an N_2O increase of nearly 25 ppb over a background of 125 ppb at 26 km near the North Pole in October. NO_y abundances are nearly 2.5 ppb greater at 40 km in the tropics than in the standard model with similarly, seasonal increases at high latitudes.

These changes have a large effect on NO_y/N_2O correlations. In the lower stratosphere (N_2O from 150 to 310 ppb) the correlation slope steepens from -0.071 to -0.088, well outside the range of observed Northern Hemisphere values (-0.069 to -0.073). Although the correlation remains tight, deviations from linearity are readily apparent in the lower stratosphere (Figure 9e).

These model results suggest that the presence of an in situ N_2O source like this [*Zellner et al.*, 1992] would have a substantial impact on stratospheric N_2O and NO_y distributions and budgets. This might not be easily ruled out from existing models and measurements given the difficulty in matching current observations [*Douglass et al.*, 1999; *Hall et al.*, 1999]. For example, differences in the profiles due to the in situ N_2O source are smaller than some of the model-model differences shown here. However, the Northern Hemisphere NO_y/N_2O correlation slope, which is relatively insensitive to model transport, constrains the maximum source strength: a *Zellner et al.* [1992] source in excess of 2 Tg N yr^{-1} gives a modeled January slope of -0.078, far outside the observed range (-0.069 to -0.073) even allowing for model uncertainties. In addition, correlations of N_2O in the summer polar regions with other source gases that do not have in situ sources such as CFCs or CH_4 could further limit such a source.

5.4. Antarctic Denitrification

Denitrification of the Antarctic polar vortex in winter has a dramatic effect on modeled Southern Hemisphere NO_y/ N_2O correlations and no noticeable effect in the Northern Hemisphere. As well as flattening the annual mean Southern Hemisphere correlation slope, the denitrification imposes a large seasonality on the slope at midlatitudes as denitrified air mixes out of the polar region in late spring.

The denitrification as modeled removes annually 0.09 Tg N of NO_y (12% of total stratospheric production). This amount appears large in proportion to the relative size of the Antarctic vortex ($\sim$ 5% of the globe), but it agrees with other estimates [*Nevison et al.*, 1997b; *Murphy and Fahey*, 1994]. Since the denitrification decreases the steepness of the Southern Hemisphere correlation slope, there is a decrease in the cross-tropopause

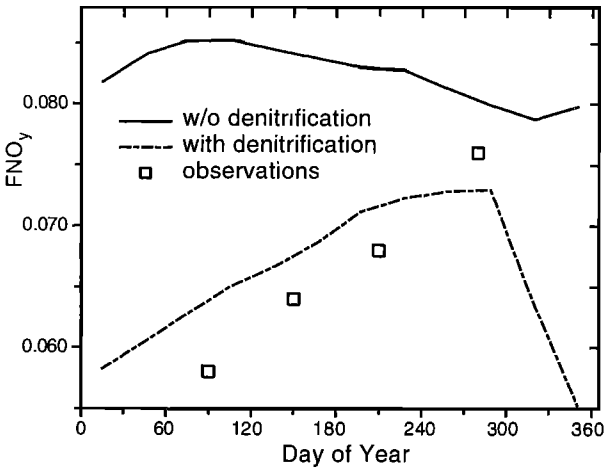

Figure 10. Modeled F_{NO_y} at 20 km versus day of year for GISS-II standard chemistry simulations with and without denitrification. Observed values are from *Nevison et al.* [1997b]. Modeled F_{NO_y} is averaged over 39°S to 55°S latitude and all longitudes.

NO_y flux carried by tracer advection in the CTM. The total NO_y flux into the troposphere (i.e., including also the sedimented NO_y from denitrification) is nearly the same as in the standard chemistry run, although it enters the troposphere in different latitudes.

The seasonal evolution of the zonally averaged F_{NO_y}, sampled at about 20 km between 39°S and 55°S, is shown in Figure 10 for model simulations with and without denitrification along with observations [*Nevison et al.*, 1997b]. Even this greatly simplified model for denitrification can explain most of the observed F_{NO_y} magnitude and seasonality.

6. Conclusions

Our results demonstrate that N_2O distributions are quite sensitive to differences in model transport, particularly the strength of the tropical upwelling in the stratosphere [e.g., *Douglass et al.*, 1999]. This has a profound impact on modeled N_2O abundances and lifetimes, which range from 115 to 173 years for the met-fields used here. These deficiencies in modeled upwelling are readily apparent through comparisons of modeled and measured N_2O profiles in the tropics. Modeled NO_y distributions are also sensitive to model dynamics. The met fields used here have sizeable differences in the location and magnitude of their NO_y maxima. Generally, the differences in N_2O and NO_y distributions resulting from different met-fields are substantially larger than the differences obtained from the alternative chemistries studied here.

Modeled NO_y/N_2O correlations, however, are much more sensitive to chemistry than transport. Hence the lower stratospheric NO_y/N_2O correlation slope provides a good test of model chemistry, being sensitive to errors in ozone abundance and temperature. With currently accepted N_2O–NO_y chemistry the modeled NO_y/N_2O

correlation slope agrees well with observations in the Northern Hemisphere. Thus one may conclude that the current understanding of stratospheric N_2O–NO_y chemistry appears to be adequate to explain current atmospheric N_2O and NO_y abundances. The large observed seasonality of the Southern Hemisphere NO_y/N_2O correlation slope at midlatitudes can only be explained by denitrification in the wintertime Antarctic vortex as noted in previous studies.

Upper stratosphere and lower mesosphere NO_y abundances depend strongly on local mesospheric NO_y chemistry, temperature, and transport. High-altitude NO_y differences among the three met-fields are comparable in magnitude to those from the alternative chemistries considered here (e.g., 10°C temperature increase, extension of mesospheric chemistry). Our conclusions are in contrast to those of *Nevison et al.* [1997a] in that the overprediction of NO_y abundances in this region could likely be due to errors in model transport and temperatures and that the photochemical model (reactions (R4) to (R7)) may be accurately modeled.

The validity of the Plumb-Ko theory, relating the lower stratospheric NO_y/N_2O correlation slope to the ratio of the fluxes, has been shown to hold in a 3-D CTM. However, the net NO_y production must be calculated from the correlation slope for N_2O between 250 and 310 ppb (i.e., -0.083) instead of the currently reported values calculated for the range of 150 to 310 ppb (i.e., -0.073).

Finally, these model studies suggest that an in situ atmospheric N_2O source such as that proposed by *Zellner et al.* [1992] would be readily observed through its impact on the NO_y/N_2O correlation slope. While a source greater than 2 Tg N yr^{-1} would be readily observed, one of magnitude less than 1 Tg N yr^{-1} would be almost impossible to detect given available measurements and current uncertainties in modeling.

This evaluation of a wide range of sensitivity studies of the stratospheric N_2O–NO_y system with 3-D models is based on the development of simplified chemistry tables (C1–C5) that accurately describe the nonlinear photochemistry of N_2O and NO_y for the monthly mean climatologies of ozone and temperature. As such, this chemistry system cannot represent the possible second-order terms that might be caused by correlated perturbations about the zone, but it should accurately represent the first-order, zonal-average production and loss rates. These tables are available from the authors.

Acknowledgments. The authors thank the anonymous reviewers for important advice and improvements to the manuscript. This work was supported by NASA's AEAP, ACMAP, and GACP programs along with the NSF Atmospheric Chemistry Program.

References

Avallone, L. M., and M. J. Prather, Tracer-tracer correlations: Three-dimensional model simulations and comparisons to observations, *J. Geophys. Res., 102,* 19,233-19,246, 1997.

Brewer, A. W., Evidence for a world circulation provided by the measurements of helium and water vapour distribution in the stratosphere, *Q. J. R. Meteorol. Soc., 75,* 351–363, 1949.

Chipperfield, M. P., Multiannual simulations with a three-dimensional chemical transport model, *J. Geophys. Res., 104,* 1781–1805, 1999.

Crutzen, P., Ozone production rates in an oxygen, hydrogen, nitrogen-oxide atmosphere, *J. Geophys. Res., 76,* 7311–7327, 1971.

Danilin, M. Y., et al., Nitrogen species in the post-Pinatubo stratosphere: Model analysis utilizing UARS measurements, *J. Geophys. Res., 104,* 8247–8262, 1999.

DeMore, W. B., S. P. Sander, D. M. Golden, R. F. Hampson, M. J. Kurylo, C. J. Howard, A. R. Ravishankara, C. E. Kolb, and M. J. Molina, Chemical kinetics and photochemical data for use in stratospheric modeling, *Eval. 12, JPL Publ. 97-4,* Jet Propul. Lab., Pasadena, Calif., 1997.

Dentener, F. J., and P. J. Crutzen, A 3-D model of the global ammonia cycle, *J. Atmos. Chem., 19,* 331-369, 1994.

Douglass, A. R., R. B. Rood, S. R. Kawa, and D. J. Allen, A three-dimensional simulation of the evolution of the middle latitude winter ozone in the middle stratosphere, *J. Geophys. Res., 102,* 19,217–19,232, 1997.

Douglass, A. R., M. J. Prather, T. Hall, S. E Strahan, P. Rasch, L. Sparling, L. Coy, and J. M. Rodriguez, Selecting the best meteorology for the global modeling initiative's assessment of stratospheric aircraft, *J. Geophys. Res., 104,* 27,545–27,564, 1999.

Fahey, D W., K. Kelly, S Kawa, A. Tuck, M. Lowenstein, K. Chan, and L. Heidt, Observations of denitrification and dehydration in the winter polar stratospheres, *Nature, 344,* 321–324, 1990.

Fahey, D. W., et al., In situ observations of NO_y, O_3, and the NO_y/O_3 ratio in the lower stratosphere, *Geophys. Res. Lett., 23,* 1653–1656, 1996.

Fang, T.-S., S. Wofsy, and A. Dalgarno, Opacity distribution functions and absorption in Schumann-Runge bands of molecular oxygen, *Planet. Space Sci., 22* 413–425, 1974.

Gunson, M. R., et al., The Atmospheric Trace Molecule Spectroscopy (ATMOS) experiment· Deployment on the ATLAS Space Shuttle missions, *Geophys. Res. Lett., 23,* 2333-2336, 1996.

Haagen-Smit, A., Chemistry and physiology of Los Angeles smog, *Ind. Eng. Chem., 44,* 1342–1346, 1952.

Hall, T., and M. J. Prather, Seasonal evolution of N_2O, O_3, and CO_2: Three-dimensional simulations of stratospheric correlations, *J. Geophys. Res., 100,* 16,699–16,720, 1995.

Hall, T. M., D. W. Waugh, K. A. Boering, and R. A. Plumb, Evaluation of transport in stratospheric models, *J. Geophys. Res., 104,* 18,815–18,839, 1999.

Hannegan, B., S. Olsen, M. Prather, X. Zhu, D. Rind, and J. Lerner, The dry stratosphere: A limit on cometary water influx, *Geophys. Res. Lett., 25,* 1649–1652, 1998.

Johnston, H., Reduction of stratospheric ozone by nitrogen oxide catalysts from supersonic transport exhaust, *Science, 173,* 517–522, 1971.

Kaminski, J. W., J. C. McConnell, and B. A. Boville, A three-dimensional chemical transport model of the stratosphere: Midlatitude results, *J. Geophys. Res., 101,* 28,731–28,751, 1996.

Keim, E. R., et al., Measurements of the NO_y–N_2O correlation in the lower stratosphere: Latitudinal and seasonal changes and model comparisons, *J. Geophys. Res., 102,* 13,193–13,212, 1997.

Kinnison, D. E., et al., The Global Modeling Initiative assessment model: Application to high-speed civil transport perturbation, *J. Geophys. Res., 106,* 1693–1712, 2001.

Koch, D. and D. Rind, $^{10}Be/^{7}Be$ as a tracer of stratospheric transport, *J. Geophys. Res., 103,* 3907–3917, 1998.

Lowenstein M., et al., New observations of the NO_y/N_2O correlation in the lower stratosphere, *Geophys. Res. Lett., 20,* 2531–2534, 1993.

McLinden, C. A., S. Olsen, B. Hannegan, O. Wild, M. J. Prather, and J. Sundet, Stratospheric ozone in 3-D models: A simple chemistry and the cross-tropopause flux, *J. Geophys. Res., 105,* 14,653–14,665, 2000.

McPeters, R., Ozone profile comparisons, in *The Atmospheric Effects of Stratospheric Aircraft: Report of the 1992 Models and Measurements Workshop*, edited by M. J. Prather and E. E. Remsberg, *NASA Ref. Publ. 1292,* D1–D37, 1993.

Michelsen, H. A., G. L. Manney, M. R. Gunson, R. Zander, Correlations of stratospheric abundances of NO_y, O_3, N_2O, and CH_4 derived from ATMOS measurements, *J. Geophys. Res., 103,* 28,347–28,359, 1998.

Minschwaner, K., and D. E. Siskind, A new calculation of nitric-oxide photolysis in the stratosphere, mesosphere, and lower thermosphere, *J. Geophys. Res., 98,* 20,401–20,412, 1993.

Minschwaner, K., G. P. Anderson, L. A. Hall, and K. Yoshino, Polynomial coefficients for calculating O_2 Schumann-Runge cross-sections at 0.5 cm^{-1} resolution, *J. Geophys. Res., 97,* 10,103-10,108, 1992.

Mosier, A., C. Kroeze, C. Nevison, O. Oenema, S. Seitzinger, and O. van Cleemput, Closing the global N_2O budget: Nitrous oxide emissions through the agricultural nitrogen cycle - OECD/IPCC/IEA phase II development of IPCC guidelines for national greenhouse gas inventory methodology, *Nutrient Cycling Agroecosystems, 52,* 225–248, 1998.

Murphy, D. M., and D. W. Fahey, An estimate of the flux of stratospheric reactive nitrogen and ozone into the troposphere, *J. Geophys. Res., 99,* 5325-5332, 1994.

Nagatani, R. M., and J E. Rosenfield, Temperature, net heating and circulation, in *The Atmospheric Effects of Stratospheric Aircraft: Report of the 1992 Models and Measurements Workshop*, edited by M. J. Prather and E. E. Remsberg, *NASA Ref. Publ. 1292,* A1–A47, 1993.

Nevison, C., S. Solomon, and R. Garcia, Model overestimates of NO_y in the upper stratosphere, *Geophys. Res. Lett., 24,* 803–806, 1997a.

Nevison, C., et al., Influence of Antarctic denitrification on two-dimensional model NO_y/N_2O correlations in the lower stratosphere, *J. Geophys. Res., 102,* 13,182–13,192, 1997b.

Nevison, C. D., E. R. Keim, S. Solomon, D. W. Fahey, J. W. Elkins, M. Loewenstein, and J. R. Podolske, Constraints on N_2O sinks inferred from observed tracer correlations in the lower stratosphere, *Global Biogeochem. Cycles, 13,* 737–742, 1999.

Nicolet, M., and S. Cieslik, The photodissociation of nitric oxide in the mesosphere and stratosphere, *Planet. Space Sci., 28,* 105–115, 1980.

Plumb, R., and M. K. Ko, Interrelationships between mixing ratios of long lived stratospheric constituents, *J. Geophys. Res., 97,* 10,145–10,156, 1992.

Prasad, S. S., Excited ozone as a possible source of atmospheric N_2O, *Nature, 289,* 386–388, 1981.

Prather, M. J., Numerical advection by conservation of second-order moments, *J. Geophys. Res., 91,* 6671–6681, 1986.

Prather, M. J., Time scale in atmospheric chemistry: Coupled perturbations to N_2O, NO_y, and O_3, *Science, 279,* 1339–1341, 1998.

Prather, M. J., M. McElroy, S. Wofsy, and J. Logan, Stratospheric chemistry: Multiple solutions, *Geophys. Res. Lett., 6,* 163–164, 1979.

Prather, M. J., M. M. Garcia, and R Suozzo, Global impact of the Antarctic ozone hole: Dynamical dilution with a three-dimensional chemical transport model, *J. Geophys. Res., 95,* 3449–3471, 1990.

Prinn, R. G., and R. Zander, Long-lived ozone-related compounds, in *Scientific Assessment of Ozone Depletion: 1998,* Rep. *44,* pp. 1.1–1.54, World Met. Org. Global Ozone Res. Mon. Proj., Geneva, 1999.

Riese, M., V. Kull, X. Tie, G. Brasseur, D. Offermann, D. Lehmacher, and A. Franzen, Modeling of nitrogen species measured by CRISTA, *Geophys. Res. Lett., 27,* 2221-2224, 2000.

Rind, D., and J. Lerner, Use of on-line tracers as a diagnostic tool in general circulation model development, 1., Horizontal and vertical transport in the troposphere, *J. Geophys. Res., 101,* 12,667–12,683, 1996.

Roche, A. E., et al., Validation of CH_4 and N_2O measurements by the CLAES instrument on the Upper Atmosphere Research Satellite, *J. Geophys. Res., 101,* 9679–9710, 1996.

Rosenfield, J., and A. Douglass, Doubled CO_2 effects on NO_y in a coupled 2-D model, *Geophys. Res. Lett., 25,* 4381–4384, 1998.

Sander, S. P., et al., Chemical kinetics and photochemical data for use in stratospheric modeling, Eval. 13, *JPL Publ. 00-003,* Jet Propul. Lab., Pasadena, Calif., 2000.

Santee, M. L., G. L. Manney, L. Froidevaux, W. G. Read, and J. W. Waters, Six years of UARS Microwave Limb Sounder HNO_3 observations: Seasonal, interhemispheric, and interannual variations in the lower stratosphere, *J. Geophys. Res., 104,* 8225–8246, 1999

Strahan, S. E., Climatologies of lower stratospheric NO_y and O_3 and correlations with N_2O based on in situ observations, *J. Geophys. Res., 104,* 30,463–30,480, 1999.

van den Broek, M. M. P., A. Bregman, and J. Lelieveld, Model study of stratospheric chlorine activation and ozone loss during the 1996/1997 winter, *J. Geophys. Res., 105,* 28,961–28,977, 2000.

Vitt, F. M., T. E. Cravens, and C. H. Jackman, A two-dimensional model of thermospheric nitric oxide sources and their contributions to the middle atmospheric chemical balance, *J. Atmos. Sol. Terr. Phys., 62,* 653–667, 2000.

Volk C. M, J. W. Elkins, D. W. Fahey, G S. Dutton, J. M. Gilligan, M Loewenstein, J. R. Podolske, K. R. Chan, and M. R. Gunson, Evaluation of source gas lifetimes from stratospheric observations, *J. Geophys. Res., 102,* 25,543–25,564, 1997

Wennberg, P. O., et al., Removal of stratospheric O_3 by radicals: In situ measurements of OH, HO_2, NO, NO_2, ClO, and BrO, *Science, 266,* 398–404, 1994.

Zellner, R., D. Hartmann, and I. Rosner, N_2O formation in the reactive collisional quenching of NO_3^* and NO_2^* by N_2, *Ber. Bunsen-Ges. Phys. Chem., 96,* 385–390, 1992.

Zipf, E. C., and S. S. Prasad, Experimental evidence that excited ozone is a source of nitrous oxide, *Geophys. Res. Lett., 25,* 4333–4336, 1998.

C. A. McLinden, Meteorological Service of Canada, 4905 Dufferin Street, Downsview, Ontario L3H 5T4, Canada. (chris.mclinden@ec.gc.ca)

S. C. Olsen, Division of Geological and Planetary Science, California Institute of Technology, Pasadena, CA 91125, USA (olsen@gps.caltech.edu)

M. J. Prather, Department of Earth System Science, University of California at Irvine, CA 92697-3100, USA. (mprather@uci.edu)

(Received February 27, 2001; revised July 3, 2001; accepted July 19, 2001.)